IOSR Journal Of Applied Physics (IOSR-JAP)
e-ISSN: 2278-4861.Volume 18, Issue 2 Ser. 1 (Mar – Apr 2026), PP 01-08
www.Iosrjournals.Org

First-Principle Investigation Of Defect-Induced Electronic State In Metal Oxide Nanowires

Dr. Vishwajeet Kumar Chandel
Assistant Teacher, Government High School (Navsthapit) Chapra Bihar

Abstract
Metal oxide nanowires have desirable properties suited to nano-electronic and spintronic devices, but are significantly affected by intrinsic defects. In this research, the electronic effect of point defects in ZnO nanowires is explored using "Density Functional Theory (DFT") and experimental characterization. Nanowires were prepared through mechanical milling, and the defects, like oxygen vacancies and interstitials, were characterized with Raman, XPS, and EPR methods. DFT calculations revealed bandgap reduction from 3.30 eV (pristine) to 2.36 eV (defective) with mid-gap states that are localized at the Fermi level. Increased ferromagnetism, which was maximized at 40 hours of milling, was explained due to higher defect concentration. The results emphasize the importance of defect engineering in controlling nanowire properties for future devices.
Keywords: *Metal oxide nanowires, DFT, Electronic, XPS*

Date of Submission: 27-02-2026 Date of Acceptance: 07-03-2026

I. Introduction

Metal oxide nanowires are one-dimensional nanomaterials that possess unique structural, electronic, and optical characteristics because of their confined geometry and high aspect ratio. The most commonly used metal oxide chemistries are semiconducting oxides, such as ZnO, TiO_2, SnO_2, and CuO [1]. Metal oxide nanowires are desirable nanoscale components for future use in nanoelectronics, sensors, energy harvesting, and photocatalysis since the quantum confinement, increased surface activity, and anisotropic charge transport provided by their unique geometry affords the nanocomponents with various solid-state possibilities [2, 3]. The ability to fabricate metal oxide nanowires through vapor-liquid-solid growth, hydrothermal methods, and chemical vapor deposition permits experimental control of size, crystallinity, and orientation [4] .

All materials have defects, but their impact becomes more significant in nanostructures because of the high surface-to-volume ratio and low dimensionality [5]. Vacancies, interstitials, and substitutional impurities are some defects that can be found in metal oxide nanowires and can create localized energy states in the bandgap, thus altering the electronic, optical, and magnetic properties of the material [6, 7]. These defects can promote or degrade device performance, depending on the type, concentration, and position of defects. For example, oxygen vacancies may function as shallow donors or trapping centers and profoundly impact charge transport and carrier lifetime [8]. Defects may also impact adsorption behavior, rendering nanowires more reactive and useful for sensing or catalysis. Hence, knowledge of and control over defects are the key to the accurate design of nanowire-based devices. A detailed exploration of these defect-induced phenomena at the atomic scale is imperative for the tailoring of material properties to address the requirements of next-generation technologies in nanoelectronics, photovoltaics, and energy storage devices [9].

The electronic transport properties of metal oxide nanowires are extremely sensitive to structural defects, which may critically change their conductive and semiconducting properties. Defects can create mid-gap states that are charge traps or recombination centers and reduce carrier mobility and the overall efficiency of the device [10]. Alternatively, some defects can increase conductivity by providing free carriers, for example, electrons from oxygen vacancies or holes from cation vacancies. In nanowires, in which quantum confinement effect further alters the band structure, even one defect can have a large effect on the density of states and Fermi level position. Such changes are of key importance in devices like field-effect transistors, photodetectors, and chemical sensors in which electrical response hinges on optimized carrier dynamics [11]. By projecting how individual defect types and distributions influence band alignment, charge localization, and transport properties, researchers may predict material performance more accurately. This requires accurate theoretical modeling to augment experimental observations [12].

First-principles approaches, and especially those which rely on "Density Functional Theory (DFT)", provide a precise and predictive means of modeling materials at the atomic scale without relying on empirical parameters [13]. First-principles methods permit the computation of important electronic properties such as band structure, "Density of States (DOS)", and charge distribution and also take into account the influence of defects, dopants, and surface reconstructions [14]. For metal oxide nanowires, first-principles simulations allow scientists to simulate ideal and defect-containing systems under a range of boundary conditions and chemical environments.

This is particularly useful for systems in which experimental characterization is difficult because of size limitations or multifaceted defect interactions. Through understanding defect formation energies, charge transition levels, and electronic structure impact, DFT-based analysis determines defect-tolerant materials and fabrication conditions. Therefore, first-principles approaches represent a foundation for comprehending and designing the functional properties of nanostructured metal oxides [15, 16].

The objective of this research is to consider the role of point defects on electronic properties of metal oxide nanowires using first-principles Density Functional Theory. This research mainly focuses on generating models of defects that resemble oxygen vacancies, metal interstitials, and substitutional atoms and examining their impacts on electronic properties such as bandgap, in-gap states, and charge carrier localization. This work will show how concentration and distribution of defects relates to atomic scale defect activity and macroscopic electronic properties and will inform the design of device applications based on metal oxide nanowires through defects.

II. Literature Review

In this section, the authors provide previous work based on first-principal investigation of defect-induced electronic state in metal oxide nanowires.

Khan et al. (2025) [17] applied DFT computations to investigate the optoelectronic and magnetic characteristics of Co-doped ZnS nanowires, both with and without structural flaws such iodine codoping, sulfur vacancy, or Zn interstitial doping. Co ions, whether interstitial or substitutional, display antiferromagnetic coupling in defect-free ZnS nanowires, according to the results. “Binding Magnetic Polarons (BMPs)” and strong ferromagnetic coupling between Co ions result from extra electron carriers interacting with the d-states of Co ions introduced by structural defects or iodine codoping.

Khan et al. (2025) [18] explored the optoelectronic, magnetic, and photocatalytic characteristics of ZnSe nanowires using first-principles computations, concentrating on iodine(I) codoping and cobalt (Co) doping. The bandgap of ZnSe nanowires, as determined by our calculations, is 3.04 eV and decreases with increasing nanowire diameter. This behavior is observed to be diameter-dependent.

Oudhia et al. (2024) [19] asserted the existence of a unique ZnO-bb structure with hitherto unreported magnetic characteristics. The O@(ZnO-bb) structure exhibits a negligible magnetic moment when Zn or O atoms are positioned at the center of ZnO-bb.

Dey et al. (2023) [20] noticed that the magnetic characteristics of GaN films varied systematically following 300 KeV Xe+ ion irradiation with various fluences, specifically 5 × 1012, 5 × 1013, and 5 × 1014 ions-cm−2. The DFT findings further demonstrate that the magnetic moment decreases for other defect configurations rather than the isolated Ga vacancies.

Nayek et al. (2023) [21] studied the framework of density functional theory, the electrical and magnetic properties of gallium vacancy (VGa) and 3d transition metal ion doped at gallium site (TMGa) in gallium oxide (β-Ga2O3). Each system has undergone Bader charge analysis in addition to band-structure computations. One potential material for spintronics applications is gallium vacancy generated β-Ga2O3.

Sumanth et al. (2022) [22] investigated the intriguing optoelectronic and spintronic properties of copper oxide, a p-type semiconductor, using both theoretical and experimental methods. As a result of its interesting absorption spectra, CuO has emerged as a promising material for broadband and near-infrared detection due to its defect-induced significant absorption in these regions.

Dive et al. (2022) [23] created the chemical process that was used in columnar nanorods of Zn0.7Mg0.3S on a commercially available glass slide. The photosensing capability and electrical investigation both verified that the produced ZnMgS films are semiconducting. Conclusion is that ZnMgS is a semiconductor with a direct bandgap, as verified by first-principles calculations.

Singh et al. (2021) [24] detailed the magnetic characteristics of 150 nm GaN films implanted with N-ions. The strain found in GaN, as determined by analysis of XRD data, indicates the presence of implanted N at interstitial points of the GaN host matrix. Furthermore, calculations based on first principles corroborate ferromagnetism as a result of Ga vacancies and the mitigation of magnetic behavior in Ga-deficient GaN through interstitial N-ion implantation.

Esquinazi et al. (2020) [25] examined the magnetic moment and magnetic order caused by specific defects in an atomic lattice of NM oxide, such as vacancies, interstitials, and nonmagnetic ions. Magnetic order at room temperature can be observed when the defect concentration is more than or equal to approximately 3 at%.

Salih et al. (2020) [26] utilized the “Atomistic ToolKit Virtual NanoLab (ATK-VNL)” program to detect molecules of hydrogen selenide (H2Se), hydrogen telluride (H2Te), and phosphine (PH3) using graphene (G) and graphene oxide with three distinct modifications (G-O, G-OH, and G-O-OH). The G-test showed that the instance of H2Te had the largest Eads, measuring -0.143 eV.

III. Research Methodology

Material Synthesis and Structural Characterization

The metal oxide nanowires were produced through high energy ball milling to form features at the nanoscale and defects. The milling occurred in argon gas to prevent oxidation of the nanopowder that had a purity of >99.9%. A planetary ball mill was used, at an operational speed of 500 rpm with 8 mm steel balls, with a ball to powder weight ratio of 10:1. The total time of milling lasted between 0 - 60 hours with periodic breaks to avoid overheating.

The structural properties of the nanowires produced were characterized by x-ray diffraction (XRD) of the Cu Kα radiation and a crystal size calculated by the Scherrer formula and Williamson-Hall plots (apparent shrinkage lines). Morphological characterization was performed by "Transmission Electron Microscopy (TEM)" and crystallinity was studied by "Selected Area Electron Diffraction (SAED)".

Defect and Compositional Analysis

To examine how defects exist in metal oxide nanowires, multiple different spectroscopic techniques were used. Raman spectroscopy was used to investigate crystallinity, phonon modes, and disorder-induced vibrational changes. The Raman spectra were analyzed by fitting Lorentzian or Gaussian functions to determine position (ω), full width at half maximum and integrated intensity (I):

$$I(w) = \frac{A}{(w - w_0)^2 + (\Gamma/2)^2}$$

Where I(ω) is the Raman intensity at frequency ω, A is peak area, w_0 is peak center and Γ is FWHM, broadening as concentration of defects increase.

Raman peak position shifts, particularly of the E_2 (high) and LO modes, were utilized to deduce bond length variation and local lattice distortion owing to defects such as oxygen vacancies and interstitials. "X-ray Photoelectron Spectroscopy (XPS)" was used to analyze the chemical states of the elements and to determine defect concentrations. The O 1s peak was deconvoluted into several components:

The relative atomic percentage of oxygen vacancies was calculated using:

$$O_V(\%) = \frac{IO_V}{IO_{total}} \times 100$$

To analyze the data define IO_V as the area under the oxygen vacancy peak, while IO_{total} represents the total area of all the O 1s deconvoluted peaks. Utilized "Electron Paramagnetic Resonance (EPR)" spectroscopy to pinpoint paramagnetic defect centers, particularly focusing on those associated with oxygen vacancies and metal vacancies. The g-factor of the EPR signal was calculated as follows:

$$g = \frac{hv}{\mu B^B}$$

Where h is Planck's constant, ν is the microwave frequency, μB is the Bohr magneton, B is the magnetic field at resonance.

Computational Methodology

DFT calculations at the first principles level were performed using the Quantum ESPRESSO package. The GGA+U method with optimized is to implement Hubbard U parameters (Ud = 8 eV for Zn 3d; Up = 8.2 eV for O 2p) to more accurately represent localized states. Supercells (3x3x2) were constructed to investigate defects (i.e., nanowires with and without point defects). Selective removal of two Zn and two O atoms representations the Zn and O vacancies. A basis set of plane waves was used with a cutoff of 480 eV and an 8x8x8 Monkhorst–Pack k-point mesh. The structural and electronic properties were assessed by performing band structures, DOS, and spin-polarized calculations, and investigating the modifications made by point defects.

Defect Modeling in Nanowires

The formation of a supercell model of size 3×3×2 based on the experimentally identified wurtzite crystal structure of ZnO was made in order to model the impact of intrinsic point defects in metal oxide nanowires. The supercell contained a total of 72 atoms and allowed for the controlled removal or addition of atoms to simulate a defect such as an oxygen vacancy, metal vacancies, and interstitials. After assembly, full geometric optimisation, to minimise total energy, was performed on all defect configurations using "Broyden–Fletcher–Goldfarb–Shanno (BFGS)" algorithm. The defect formation energy was defined as

$$E_{form} = E_{defect} - E_{perfect} + \sum_i n_i \mu_i$$

Where E_{defect} equals to total energy of the defective supercell, $E_{perfect}$ is total energy of the perfect supercell, n_i number of atoms added or removed and μ_i chemical potential of species.

Electronic Structure and Density of States Calculations

Band structure and DOS calculations were carried out on perfect and defective nanowires using spin-polarized DFT+U. Electronic band structure was calculated along high-symmetry directions within the Brillouin zone using an 8×8×8 Monkhorst–Pack k-point grid.

The bandgap was determined from the energy gap between the "Conduction Band Minimum (CBM)" and "Valence Band Maximum (VBM)":

$$E_g = E_{CBM} - E_{VBM}$$

To dive deeper into the contributions from Zn 3d, O 2p, and defect-induced states, derived the "Total Density of States (TDOS)" and the Partial Density of States (PDOS)". This analysis was crucial in pinpointing the mid-gap states that defects introduce, as well as their tendency to localize near the Fermi level. To back up our findings, calculate the bandgap of pristine ZnO nanowire, which came out to be around 3.30 eV.

Convergence Testing and Parameter Validation

Convergence tests are conducted to ensure both the numerical accuracy and efficiency of our calculations. To verify the total energy convergence in relation to the plane-wave cutoff energy, we used the following method:

$$\Delta E_{cutoff} = |E_{n+1} - E_n| < 0.01 eV/atom$$

The energy cutoff was set to 480 eV after testing values from 300 to 600 eV. The k-point grid was also set between 4×4×4 and 8×8×8, selecting the grid based on total energy stability and all other calculations were kept constant. Also, in the direction perpendicular to the wire axis vacuum spacing of at least 15 Å was maintained to minimize the possibility of inter-wire interactions due to periodic boundary conditions being used. The DFT+U method was used to account for the systematic underestimation of bandgap found in normal DFT. The final values used were:

$$U_{Zn} = 8.0eV, \quad U_0 = 8.2eV$$

These values were optimized to reproduce the experimental lattice constants and bandgap, ensuring high fidelity in electronic structure modeling.

IV. Result And Analysis

Vibrational Analysis: Raman Spectroscopy

The Raman spectra presented the characteristic E2(high), A1(LO) and E1(LO) modes. Upon increases to milling time, the E2(high) peak at ~438 cm^{-1} reduced intensity, broadened in the asymmetric and showed an increase in defects and reduced crystallinity. However, the A1(LO) and E1(LO) modes, related to defects, became more apparent and showed red-shifts. The red-shifting, which can show signs of phonon softening, is a pearl to bond strength and lattice disorder due to defects (most notably oxygen vacancies and zinc interstitial defects).

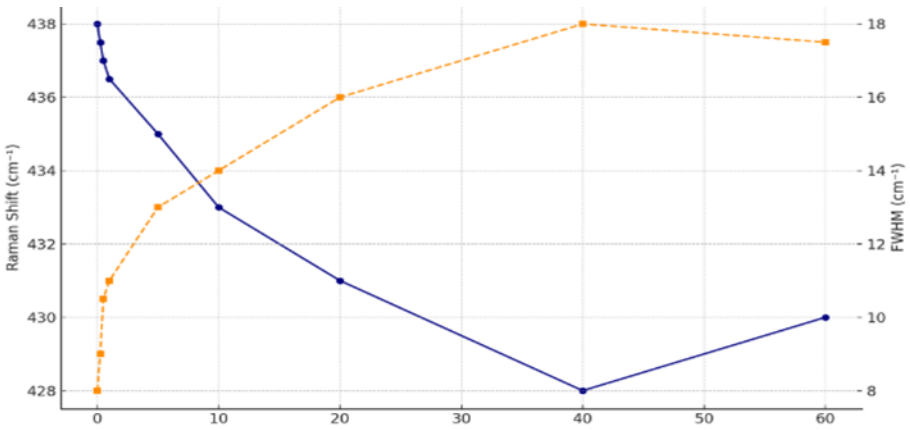

Figure 1: Raman E_2(high) peak shift and FWHM variation with time

This plot shows the development of the Raman E_2(high) vibrational mode and FWHM as functions of milling time in the course of synthesizing metal oxide nanowires. The E_2(high) peak is first seen at ~438 cm^{-1} corresponding to a very crystalline lattice. At the same time, FWHM rises from ~8 cm^{-1} to ~18 cm^{-1}, reflecting phonon lifetime broadening, which has a direct correlation with the incorporation of structural defects and degradation of long-range order of the nanowire lattice.

Chemical Composition and Defect Identification: XPS

X-ray Photoelectron Spectroscopy (XPS) showed the chemical composition, and point defect states in the nanowires. The O 1s peak was deconvoluted into three components: O_latt (~530 eV) (oxygen atoms in lattices), O_V (~532 eV) (oxygen atoms in vacancies), and O_C (~534 eV) (oxygen atoms on the surface or bonded with other molecules). The O_V component increased significantly with milling time, indicating an increase in corresponding point defects. The Zn 2p spectra did not show any variation, indicating that the Zn was in the +2 oxidation state.

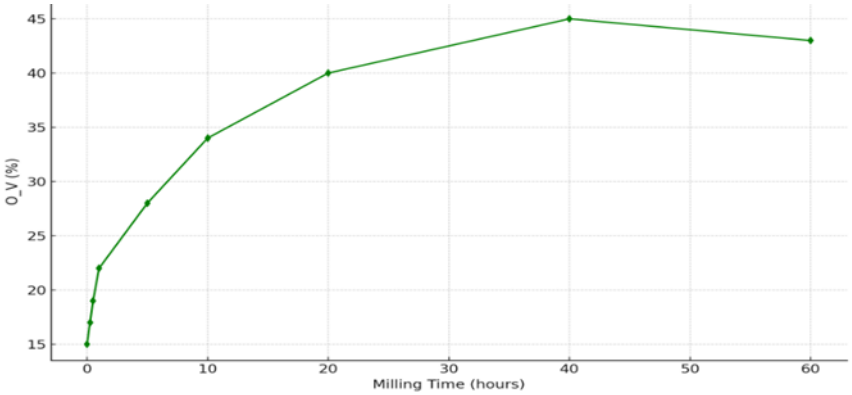

Figure 2: "Increase in Oxygen Vacancy Concentration with Milling Time

The graph illustrates how the concentration of oxygen vacancies in metal oxide nanowires changes with milling time, based on the deconvolution of the XPS O 1s peak. The climbs steadily from about 15% in the original sample to a peak of around 45% after 40 hours. The slight decrease observed at 60 hours might suggest some level of defect recombination or saturation effects.

Detection of Defect Centers: EPR Analysis

"Electron Paramagnetic Resonance (EPR)" spectra indicated an intense signal at g ~ 1.95, typical of unpaired electrons within oxygen vacancy sites. On increasing the milling time, the intensity of the EPR signal increased, indicating an enhancement in the concentration of paramagnetic defect centers. Annealing the samples diminished the EPR signal, ascertaining the healing of defects to some extent.

Table 1: EPR Signal Intensity with the Milling Time

Milling Time (h)	EPR Intensity (a.u.)
0.00	10
0.25	15
0.50	20
1.00	28
5.00	40
10.00	55
20.00	68
40.00	75
60.00	70

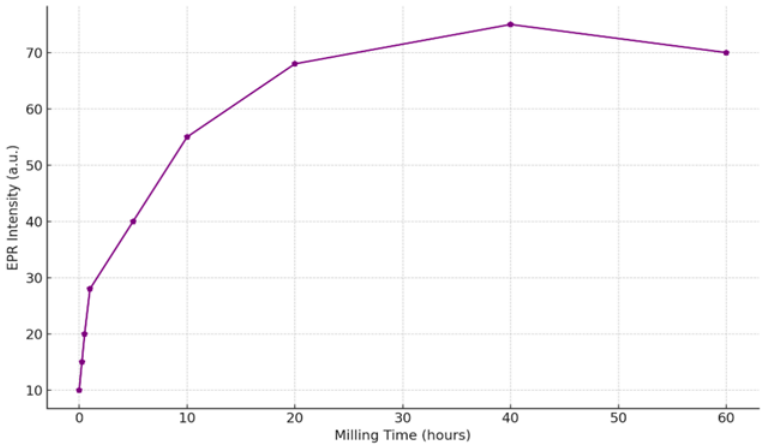

Figure 3: EPR Signal Intensity with Milling Time

The plot is the variation of EPR signal intensity with milling time for metal oxide nanowires, as monitored at a g-factor of about 1.95, typical for oxygen vacancy-related paramagnetic centers. As the milling time goes up, the EPR intensity increases substantially, reflecting the increased concentration of unpaired electrons related to defect centers, particularly oxygen vacancies. The intensity maximum occurs at 40 hours, in agreement with the highest defect density

Magnetic Behavior and Defect-Induced Ferromagnetism

Magnetic measurements clearly shown a transition from weak paramagnetism in pristine nanowires, to distinct ferromagnetism in the milled samples. The saturation magnetization and coercivity captured in the magnetic measurements should increase with milling time, and reached a maximum around 40 hours. This increase is thought to result from the increase in the concentration of oxygen vacancies and zinc interstitials defects, which both contribute localized moments and also lead to long range ferromagnetic ordering.

At 60 hours of milling, a slight decrease in magnetization was found in the mld (6) - and it not likely related in sample defects or elemental weight change since other studies report higher values - probably due to defect recombination or as a result of partial grain growth that decrease available number of active magnetic sources. The temperature dependent magnetization loops confirmed there was ferromagnetism at room temperature. All of the experimental results were backed up by supporting studies through EPR and XPS; which together clearly still encouragingly shows that controlling the introduction of defects by way of ball milling is a respective approach to introducing and further tuning the ferromagnetic behaviour of non-magnetic metal oxide nanowires.

Electronic Structure and Bandgap Engineering

Using first-principles DFT calculations, the pristine ZnO nanowires exhibited a direct bandgap of 3.30 eV in the absorption spectra. In contrast, the bandgap decreased to 2.36 eV upon introducing oxygen and metal vacancies in a 3 × 3 × 2 supercell. This decrease in the bandgap occurred due to mid-gap states introduced by defects. The DOS demonstrated that the in-gap states were mainly contributed to by O 2p and Zn 3d orbitals. The spin asymmetry present in the DOS indicates the possibility of magnetic polarization.

Table 2: Crystallite Size and Bandgap vs. Milling Time

Milling Time (h)	Crystallite Size (nm)	Bandgap (eV)
0.00	50.66	3.30
0.25	32.30	3.30
0.50	26.16	3.30
1.00	22.14	3.30
5.00	14.68	3.00
10.00	14.41	2.80
20.00	14.10	2.60
40.00	14.04	2.36
60.00	14.07	2.40

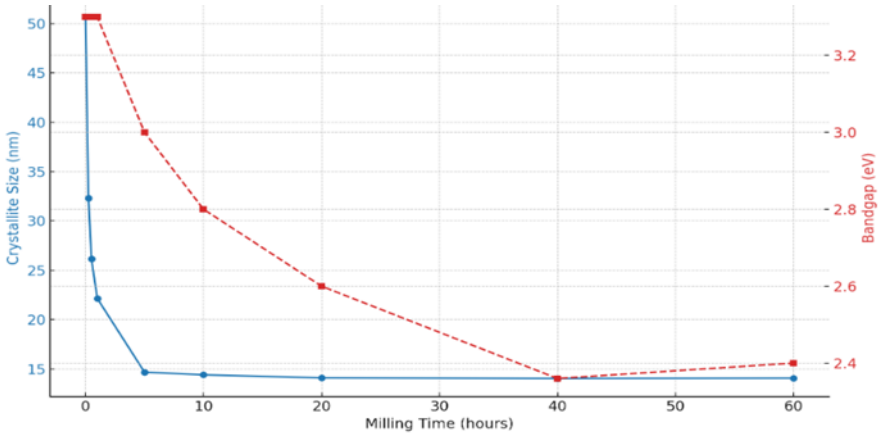

Figure 4: Variation of Crystallite Size and Bandgap with Milling Time

The graph indicates that crystallite size and bandgap energy vary with milling time. The blue line is the crystallite size, which decreases very steeply in the initial approx. 5 hours of milling but then levels off, indicating there must be some maximum size below which the grains can no longer decrease. Contrarily, the bandgap energy, as indicated by the red dashed line, decreases gradually, particularly after 10 hours of milling. This is a result of the increase in defect states generated by defects, which alter the electronic structure.

V. Conclusion

This thorough exploration of defect-generated electronic states in metal oxide nanowires, using both experimental and first-principles methods, emphasizes the pivotal role played by intrinsic point defects in controlling the material's structural, electronic, and magnetic properties. The formation of such defects as oxygen vacancies and metal interstitials, especially via mechanical ball milling, heavily modifies the nanowire's crystallinity, decreases bandgap energy from 3.30 eV to 2.36 eV, and creates mid-gap states affecting charge localization and transport. Electron paramagnetic resonance and magnetic measurements affirmed that the defects also create room-temperature ferromagnetism, which peaks at 40 hours of milling. DFT computations confirmed these findings, displaying defect-related changes in the spin polarization and density of states. The consistency between theory and experiment not only demonstrates the promise of defect engineering in designing the functional response of nanowires but also forms the foundation for the design of next-generation nanodevices with improved optoelectronic and spintronic characteristics.

Reference

[1] Devan, Rupesh S., Ranjit A. Patil, Jin-Han Lin, And Yuan-Ron Ma. "One-Dimensional Metal-Oxide Nanostructures: Recent Developments In Synthesis, Characterization, And Applications." Advanced Functional Materials 22, No. 16 (2012): 3326-3370.

[2] Tonezzer, Matteo, Dang Thi Thanh Le, Lai Van Duy, Nguyen Duc Hoa, Flavia Gasperi, Nguyen Van Duy, And Franco Biasioli. "Electronic Noses Based On Metal Oxide Nanowires: A Review." Nanotechnology Reviews 11, No. 1 (2022): 897-925.

[3] Rackauskas, Simas, Albert G. Nasibulin, Hua Jiang, Ying Tian, Victor I. Kleshch, Jani Sainio, Elena D. Obraztsova, Sofia N. Bokova, Alexander N. Obraztsov, And Esko I. Kauppinen. "A Novel Method For Metal Oxide Nanowire Synthesis." Nanotechnology 20, No. 16 (2009): 165603.

[4] Klamchuen, Annop, Masaru Suzuki, Kazuki Nagashima, Hideto Yoshida, Masaki Kanai, Fuwei Zhuge, Yong He Et Al. "Rational Concept For Designing Vapor–Liquid–Solid Growth Of Single Crystalline Metal Oxide Nanowires." Nano Letters 15, No. 10 (2015): 6406-6412.-

[5] Rafique, Muhammad, Muhammad Bilal Tahir, Muhammad Shahid Rafique, Neelam Safdar, And Rabia Tahir. "Nanostructure Materials And Their Classification By Dimensionality." In Nanotechnology And Photocatalysis For Environmental Applications, Pp. 27-44. Elsevier, 2020.

[6] Raizada, Pankaj, Vatika Soni, Abhinandan Kumar, Pardeep Singh, Aftab Aslam Parwaz Khan, Abdullah M. Asiri, Vijay Kumar Thakur, And Van-Huy Nguyen. "Surface Defect Engineering Of Metal Oxides Photocatalyst For Energy Application And Water Treatment." Journal Of Materiomics 7, No. 2 (2021): 388-418.

[7] Punia, Khushboo, Ganesh Lal, Satya Narain Dolia, And Sudhish Kumar. "Defects And Oxygen Vacancies Tailored Structural, Optical, Photoluminescence And Magnetic Properties Of Li Doped Zno Nanohexagons." Ceramics International 46, No. 8 (2020): 12296-12317.

[8] Janotti, Anderson, And Chris G. Van De Walle. "Oxygen Vacancies In Zno." Applied Physics Letters 87, No. 12 (2005).

[9] Fonseka, H. A., N. Denis, J. A. Gott, X. Yuan, R. Beanland, H. H. Tan, C. Jagadish, A. M. Sanchez, And M. De Luca. "Revealing Inclined Twin Related Defects In III–V Nanowires Grown In Popular Alternative Crystallographic Directions." The Journal Of Physical Chemistry C 128, No. 50 (2024): 21593-21603.

[10] Anta, Juan A. "Electron Transport In Nanostructured Metal-Oxide Semiconductors." Current Opinion In Colloid & Interface Science 17, No. 3 (2012): 124-131.

[11] Mishra, Raghvendra Kumar, And Kartikey Verma. "Defect Engineering In Nanomaterials: Impact, Challenges, And Applications." Smart Materials In Manufacturing 2 (2024): 100052.

[12] Klein, Andreas. "Energy Band Alignment At Interfaces Of Semiconducting Oxides: A Review Of Experimental Determination Using Photoelectron Spectroscopy And Comparison With Theoretical Predictions By The Electron Affinity Rule, Charge Neutrality Levels, And The Common Anion Rule." Thin Solid Films 520, No. 10 (2012): 3721-3728.

[13] Pandit, Bidhan, Sachin R. Rondiya, Shoyebmohamad F. Shaikh, Mohd Ubaidullah, Ricardo Amaral, Nelson Y. Dzade, Emad S. Goda, Harjot Singh Gill, And Tokeer Ahmad. "Regulated Electrochemical Performance Of Manganese Oxide Cathode For Potassium-Ion Batteries: A Combined Experimental And First-Principles Density Functional Theory (DFT) Investigation." Journal Of Colloid And Interface Science 633 (2023): 886-896.

[14] Anthore, Anne, Hugues Pothier, And Daniel Esteve. "Density Of States In A Superconductor Carrying A Supercurrent." Physical Review Letters 90, No. 12 (2003): 127001.

[15] Wang, Hui, Yufang Wang, Xuewei Cao, Lei Zhang, Min Feng, And Guoxiang Lan. "Simulation Of Electronic Density Of States And Optical Properties Of Pbb4o7 By First-Principles DFT Method." Physica Status Solidi (B) 246, No. 2 (2009): 437-443.

[16] Wang, Hui, Yufang Wang, Xuewei Cao, Lei Zhang, Min Feng, And Guoxiang Lan. "Simulation Of Electronic Density Of States And Optical Properties Of Pbb4o7 By First-Principles DFT Method." Physica Status Solidi (B) 246, No. 2 (2009): 437-443.

[17] Khan, Muhammad Sheraz, And Bingsuo Zou. "A First-Principles Study Of N-Type Defects And Cobalt Doping On Magnetic And Optical Properties Of Zns Nanowires: Implications For Spintronic And Photovoltaic Applications." The Journal Of Physical Chemistry C 129, No. 13 (2025): 6486-6501.

[18] Khan, Muhammad Sheraz, Dan Luo, And Bingsuo Zou. "Magnetic And Optoelectronic Properties Of Cobalt And Iodine Doping In Znse Nanowires For Spintronic And Water-Splitting Applications: A First-Principles Investigation." ACS Applied Nano Materials (2025).

[19] Oudhia, Anjali, Sakshi Sharma, Ashok Kumar Shrivastav, Renu Kumari, And Mohan L. Verma. "Ab Initio Investigation Of Magnetic Properties Of Metal Doped Zno-Buckyball Structures." Journal Of Magnetism And Magnetic Materials 589 (2024): 171579.

[20] Dey, Sharmistha, Preetam Singh, Vikash Mishra, Neetesh Dhakar, Sunil Kumar, Fouran Singh, Pankaj Srivastava, And Santanu Ghosh. "Role Of Position Specific Ga And N Vacancy Related Defects By Ion Irradiation In Tailoring The Ferromagnetic Properties Of Thin Gan Films: An Experimental And First Principle-Based Study." Solid State Communications 371 (2023): 115232.

[21] Nayek, Apurba Kumar, Sudipta Moshat, Dirtha Sanyal, And Mahuya Chakrabarti. "Magnetic Properties Of Defect Induced B-Ga2O3: A First Principles Study." Computational Condensed Matter 35 (2023): E00810.

[22] Sumanth, Arige, Vikash Mishra, Poonam Pandey, MS Ramachandra Rao, And Tejendra Dixit. "Investigations Into The Role Of Native Defects On Photovoltaic And Spintronic Properties In Copper Oxide." IEEE Transactions On Nanotechnology 21 (2022): 522-527.

[23] Dive, Avinash S., Jitendra S. Kounsalye, And Ramphal Sharma. "Growth, Structural, Morphological, Opto-Electrical And First-Principle Investigations Of Znmgs Thin Films." Journal Of Materials Science: Materials In Electronics 33, No. 23 (2022): 18798-18806.
[24] Singh, Preetam, Santanu Ghosh, Vikash Mishra, Sajal Barman, Sudipta Roy Barman, Arvind Singh, Sunil Kumar, Zichao Li, Ulrich Kentsch, And Pankaj Srivastava. "Tuning Of Ferromagnetic Behavior Of Gan Films By N Ion Implantation: An Experimental And First Principle-Based Study." Journal Of Magnetism And Magnetic Materials 523 (2021): 167630.
[25] Esquinazi, Pablo David, Wolfram Hergert, Markus Stiller, Lukas Botsch, Hendrik Ohldag, Daniel Spemann, Martin Hoffmann Et Al. "Defect-Induced Magnetism In Nonmagnetic Oxides: Basic Principles, Experimental Evidence, And Possible Devices With Zno And Tio2." Physica Status Solidi (B) 257, No. 7 (2020): 1900623.
[26] Salih, Ehab, And Ahmad I. Ayesh. "First Principle Investigation Of H2Se, H2Te And PH3 Sensing Based On Graphene Oxide." Physics Letters A 384, No. 29 (2020): 126775.